



OPEN

SF3B4 downregulation restrains lung adenocarcinoma tumorigenesis via 5' alternative splicing of KAT2A

Ailin Qu¹, Bo Han², Mengmeng Hua^{3,4}, Chune Wang^{3,4} & Tao Li⁵✉

Aberrant expression of splicing factors, including SF3B4, plays a vital role in lung adenocarcinoma (LUAD). However, the impact of SF3B4 in the progression of LUAD has not been studied well. Here, we demonstrated the effects of SF3B4 in LUAD via apoptosis, proliferation, migration assays, etc. Gene manipulations confirmed the role of SF3B4 via KAT2A. SF3B4 was found to promote LUAD growth. Further studies found that, upon SF3B4 knockdown in LUAD cells, an alternative splice site occurred at the 5'-UTR of KAT2A, which led to the downregulation of KAT2A at both RNA and protein levels. Furthermore, the decrease in KAT2A expression partially reversed the effect of SF3B4 in promoting tumorigenesis. The axis SF3B4/ KAT2A was identified as a significant player in LUAD progression, shedding light on the therapeutic development in LUAD.

Abbreviations

AS	Alternative splicing
CBTCCAS	Cell Bank of Type Culture Collection of Chinese Academy of Sciences
CPTAC	Clinical Proteomic Tumor Analysis Consortium
DEGs	Differentially expressed genes
FBS	Fetal bovine serum
GAPDH	Glyceraldehyde 3-phosphate dehydrogenase
GEO	Gene Expression Omnibus
GEPIA	Gene Expression Profiling Interactive Analysis
GTEX	Genotype-Tissue Expression
KAT2A	Lysine acetyltransferase 2A
KLF4	Krüppel-like factor 4
LUAD	Lung adenocarcinoma
mRNA	Messenger ribonucleic acid
OS	Overall survival
PFS	Progression-free survival
PTPMT1	Protein tyrosine phosphatase mitochondrial 1
PVDF	Polyvinylidene fluoride
RBMBA	Rugosity and biofilm structure modulator A
RT-PCR	Reverse transcription-polymerase chain reaction
SF3B4	Splicing factor 3B subunit 4
siRNA	Short interfering RNA
snRNA	Small nuclear RNA
snRNP	Small nuclear ribonucleoproteins
SPAG5	Sperm-associated antigen 5
SRSF1	Serine/arginine-rich splicing factor 1

¹Department of Clinical Laboratory, Qilu Hospital, Shandong University, Jinan 250012, Shandong, China. ²Department of Pathology, Qilu Hospital, Cheeloo College of Medicine, Shandong University, Jinan, Shandong, China. ³Department of Oral and Maxillofacial Surgery, Qilu Hospital of Shandong University, Jinan, Shandong, China. ⁴Institute of Stomatology, Shandong University, Jinan, Shandong, China. ⁵Department of Respiratory Diseases, Qilu Hospital of Shandong University, No. 107, Culture West Road, Jinan, China. ✉email: litao@qiluhospital.com; Qllitao@126.com

TCGA The Cancer Genome Atlas
UTR Untranslated region

Lung adenocarcinoma (LUAD) is the most common subtype of non-small cell lung cancer (NSCLC), with a high incidence rate and low survival time¹. Despite progress in surgical methods and therapeutic targets over the past years, no evident improvement has been achieved in the survival of LUAD patients². This is primarily attributed to the complications associated with diverse mutations in LUAD. Hence, this unmet need creates a strong drive to uncover the mechanisms underlying the development of LUAD to improve patient outcomes.

Alternative splicing (AS) produces different mRNA splicing isomers from an mRNA precursor through different splicing methods. This produces isoforms of mRNA and protein variants from a single gene³, leading to different structural and functional properties in final protein products. Abnormal AS was shown to cause cancer^{4,5}, and regulate cancer progression^{6,7}. For example, SRSF1, a splicing factor, alternates the splicing of PTPMT1, regulating the resistance to radiotherapy in LUAD⁸.

RNA splicing is modulated by two spliceosomes, of which the major one functions through U2 snRNP, a particle consisting of the splicing factors SF3a, SF3b, and U2 snRNA⁹. SF3B4 is one of the SF3b complex components¹⁰. The SF3B4 haploinsufficiency or mutation was reported to be a major genetic factor that caused Nager syndrome¹¹. Notably, dysregulation of SF3B4 expression has been implicated in multiple tumors. The expression of SF3B4 was shown to be increased in hepatocellular carcinoma compared to that in normal tissues^{12,13}. In LUAD, Kim H reported that SF3B4 depletion slowed down the growth of LUAD cells via Ubiquitination factor E4B-mediated expression of p53/p21 and p27¹⁴. However, the research on the relationship between SF3B4 and LUAD is only at the beginning stage, especially on the effect and mechanism of SF3B4 alternative splicing on LUAD has not been studied well.

Here, we found that SF3B4 protein was upregulated in LUAD patients and played the role of oncogenes in the proliferation, migration, and invasion of LUAD. In addition, our results reveal that SF3B4 regulated LUAD progression via the alternative splicing of KAT2A for the first time.

Results

Aberrant expression of SF3B4 in LUAD

To search critical splicing factors involved in LUAD, overlapping analysis of 2562 upregulated genes and 134 core splicing factors revealed 15 potential candidates, including RBM8A, LSM8, and SF3B4 (Fig. 1A,B). To explore the effects of SF3B4 in LUAD, we examined the mRNA profile of SF3B4 in LUAD and normal lung tissues from the GTEx and TCGA databases (Fig. 1C). Then, we investigated the expression of SF3B4 protein in LUAD and normal lung tissues from the CPTAC database (Fig. 1D). Notably, the mRNA level of SF3B4 was higher in LUAD tissues and LUAD cells than in normal samples (Fig. 1E,F). These findings were further confirmed by comparing the results from the staining of SF3B4 in human tumor tissues to those in healthy tissues (Fig. 1G).

We performed a Kaplan–Meier analysis to explore whether SF3B4 contributed to LUAD progression. We observed that patients with high levels of SF3B4 had worse overall survival (OS) and poor progression-free survival (PFS) (Fig. 1H,I). Next, correlations of SF3B4 to clinicopathological features were analyzed. Importantly, SF3B4 expression was substantially correlated with the TNM stage (Table 1) in LUAD.

Promoting the role of SF3B4 in LUAD

To explore the role of SF3B4 in LUAD, we transfected siRNA targeting SF3B4 into wild-type LUAD cells. The efficiency of SF3B4 knockdown was validated in transcription and translation levels (Fig. 2A). SF3B4 knockdown significantly suppressed the proliferation of LUAD cells (Fig. 2B,D). Besides, SF3B4 knockdown significantly inhibited the formation of colonies derived from A549 and H1650 cells, respectively (Fig. 2E). Furthermore, we found that the knockdown of SF3B4 decreased the capacity to migrate and invade LUAD cells (Fig. 2F,G). Consistently, the knockdown of SF3B4 inhibited the capacity of LUAD cells in wound healing (Fig. 2H). Furthermore, we showed that SF3B4 knockdown induced apoptosis in LUAD cells in vitro (Fig. 2C, Supplementary Fig. 1). These data suggest that targeting SF3B4 could be an effective treatment for LUAD.

SF3B4 promotes LUAD tumor growth

To examine the effects of SF3B4 in vivo, we constructed the cell lines with a knockdown of SF3B4 and a cell line with a control vector. We subcutaneously inoculated sh-SF3B4 and sh-Ctrl cells in mice. After 3 weeks, we found dramatic decreases in tumor size and weights from the mice-bearing tumors derived from SF3B4 knockdown cells compared to the control (Fig. 3A–C). Besides, we quantified the levels of SF3B4 and Ki-67 with immunohistochemical staining in this nude mouse xenograft model. The level of SF3B4 was reduced in the SF3B4 knockdown group (Fig. 3D). The intensity of Ki-67 was lower in tumors derived from SF3B4 knockdown cells than that derived from control (Fig. 3D). In summary, the results demonstrated a promoting role of SF3B4 on LUAD.

KAT2A is an essential downstream effector of SF3B4

RNA-seq was performed in A549 cells with or without SF3B4 knockdown to explore the pathway through which SF3B4 drove the growth and development of LUAD. The profile of differentially expressed genes (DEGs) was plotted (Fig. 4A,B). We found 324 upregulated and 597 downregulated genes. Gene analysis was performed to depict the biological functions of these DEGs. Interestingly, the enriched biological pathways are involved in regulating the cell cycle and the negative regulation of phase transitions in the mitotic cell cycle (Fig. 4C). Exploring the genes that are down-regulated after SF3B4 knockdown could provide valuable insights. For downregulated genes upon SF3B4 knockdown, the enrichment of biological pathways was DNA double-strand break repair, cell cycle regulation, and DNA replication in downregulated genes (Fig. 4E). Interestingly, 23 genes were identified to have

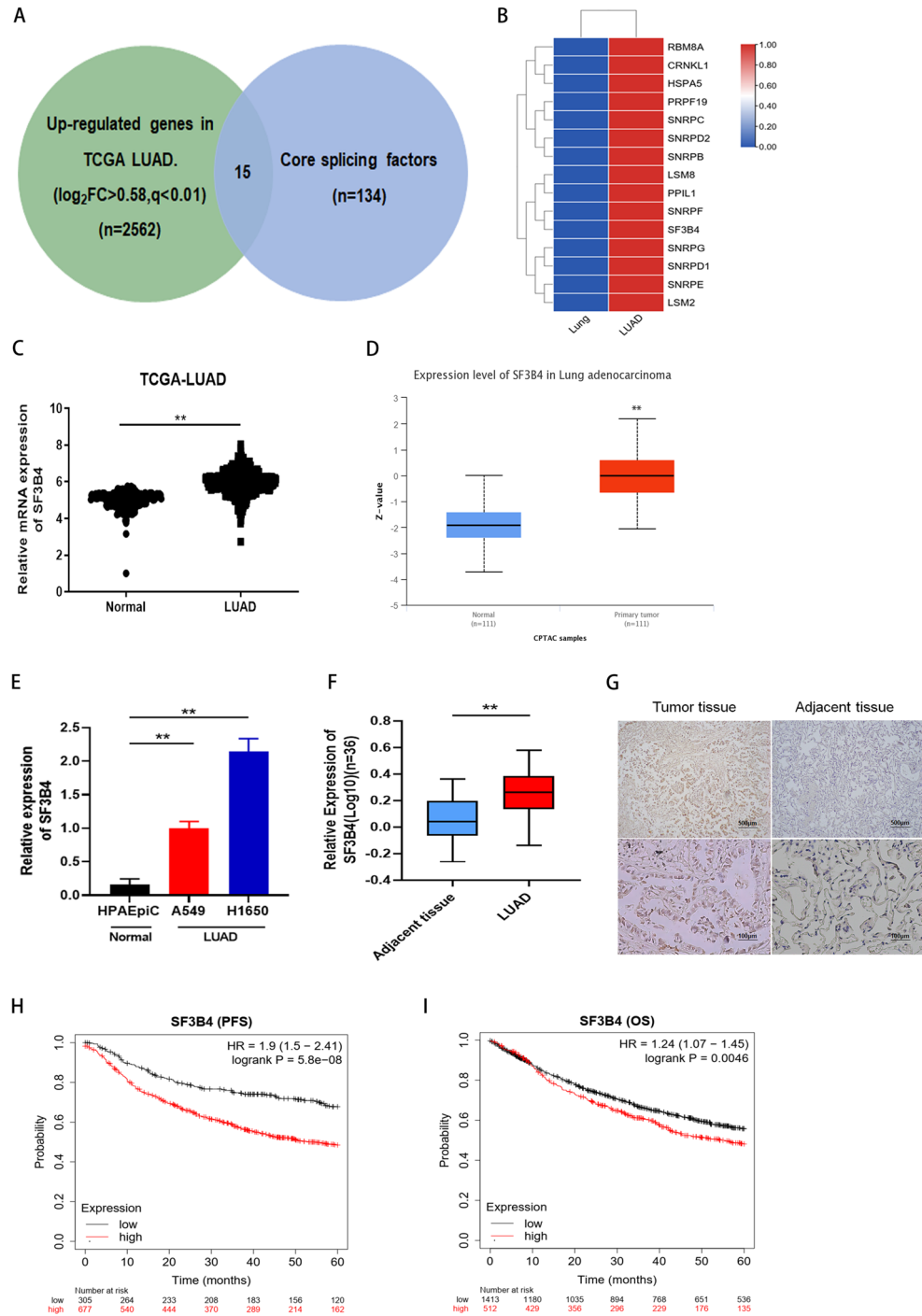


Figure 1. Aberrant expression of SF3B4 in LUAD. **(A)** Venn diagram showing the 15 genes correlated with upregulated genes in TCGA LUAD (n = 2562) and involved in core splicing genes (n = 134). **(B)** Heatmap of selected genes in **(A)**. **(C)** Relative mRNA expression of SF3B4 in LUAD and normal lung tissues from GTEx and TCGA and database. **(D)** Expression of SF3B4 protein in LUAD and normal lung tissues from CPTAC database. **(E)** SF3B4 mRNA levels in A549, H1650, and HPAEpiC cells, measured by qRT-PCR. **(F)** SF3B4 mRNA level in human lung tissues (n = 36), analyzed by qRT-PCR. **(G)** IHC staining of SF3B4 in human LUAD tissues and corresponding healthy tissues. **(H,I)** Kaplan–Meier analysis on the effects of SF3B4 on PFS and OS of LUAD patients. * $P < 0.05$, ** $P < 0.01$.

both downregulated expressed genes and were involved in the differential AS events in A549 cells (Fig. 4D). We then performed visual analysis on the identified genes, and rMATs found that the 5' end of KAT2A had

Variable	Case No. (%)	SF3B4 expression		P-value
		Low (n = 12)	High (24)	
Gender				
Male	22 (61.1%)	6	16	0.472
Female	14 (38.9%)	6	8	
Age (years)				
≤ 60	17 (47.2%)	5	12	0.732
> 60	19 (52.8%)	7	12	
Smoking history				
Yes	20 (55.6%)	8	12	0.482
No	16 (44.4%)	4	12	
Differentiation				
Poor	27 (75.0%)	9	18	0.999
Moderate/well	9 (25.0%)	3	6	
TNM stage				
I/II	17 (47.2%)	9	8	0.032
III	19 (52.3%)	3	16	

Table 1. Clinicopathological variables and SF3B4 expression in LUAD patients (n = 36).

variable splicing. An A5SS variable splicing event occurred in the annotated region of the shadow. When SF3B4 expression is interfered with si-SF3B4, a long exon is generated at the 5' variable splicing site of KAT2A. This results in the transcription containing the long exon no longer encoding. This reduces the expression of KAT2A protein. (Fig. 4F). To further explore the role of SF3B4 in regulating KAT2A, the changes in the KAT2A level were confirmed by qRT-PCR and Western blotting upon SF3B4 knockdown in LUAD cells, including A549 and H1650. Both mRNA and protein levels of KAT2A were significantly downregulated upon SF3B4 knockdown (Fig. 4G,H). These results suggest that KAT2A is a target of SF3B4 in LUAD.

SF3B4 leads to AS of KAT2A

We further analyzed the splice variants of KAT2A mRNA with an ensemble genome browser to explore if SF3B4 regulated the levels of KAT2A through AS. We found that a long exon was produced in the unspliced transcript of KAT2A-202, different from the spliced transcript of KAT2A-201 (Fig. 5A). KAT2A-201 mRNA level was increased than that of KAT2A-202 in LUAD cells. Furthermore, we analyzed the levels of KAT2A-201 and KAT2A-202 transcripts from both LUAD tissues and normal controls in TCGA and GTEx databases. We found that the expression of KAT2A-201 transcripts in LUAD was relatively higher than that of KAT2A-202, while KAT2A-202 was relatively higher in normal lung tissue (Fig. 5B). RT-PCR results verified the changes in the levels of KAT2A-201 and KAT2A-202. We observed that upon SF3B4 knockdown, the level of the unspliced transcript variant was significantly increased, and that of the spliced transcript variant was significantly reduced (Fig. 5C,D). Interestingly, RIP-PCR data showed that the mRNA level of KAT2A in SF3B4 precipitates was significantly increased than that in the IgG group (Fig. 5E). This suggests that SF3B4 regulates the KAT2A via A5SS.

Targeting KAT2A in LUAD

To evaluate the role of KAT2A alone in LUAD cells, we transiently silenced KAT2A with siRNA transfection into LUAD cells. The knockdown of KAT2A was confirmed (Fig. 6A,B). The analyses revealed that KAT2A knockdown decreased cell viability and colony formation and increased cell apoptosis (Fig. 6C–F, Supplementary Fig. 2). Transwell analysis results showed that knockdown of KAT2A reduced the invasion and migration capacities of LUAD cells (Fig. 6G–H).

Furthermore, rescue experiments were performed to confirm the effect of KAT2A in SF3B4-regulated malignancy of LUAD. We transfected si-NC or KAT2A-targeted siRNA into LUAD cells with SF3B4 overexpression (Fig. 7A,B). We observed that proliferation rate, migration, and invasion capacities in LUAD cells enhanced with SF3B4 overexpression were impaired upon the KAT2A knockdown (Fig. 7C–F). These findings suggest the effects of KAT2A in the SF3B4-modified oncogenesis of LUAD.

Discussion

Emerging evidence has manifested that splicing factor SF3B4 binds to U2 snRNP, which regulates the AS of premature mRNA¹⁵. SF3B4 is an oncogenic driver in multiple tumor types. However, it is a tumor-suppressor in pancreatic cancer^{16–19}. We showed increased levels of SF3B4 in LUAD tissues and cells. The upregulated level of SF3B4 was associated with a poor prognosis of LUAD. Furthermore, we observed that SF3B4 knockdown suppressed proliferation and mobility and induced apoptosis in LUAD cells. Meanwhile, we proved that the SF3B4 knockdown slowed tumor growth in a mouse model. Our investigation showed that SF3B4 exhibited oncogenic properties in LUAD, in line with other studies¹⁴.

Understanding the underlying mechanisms of SF3B4 as an oncogene requires further studies. In cervical cancer, Li et al. proposed that the knockdown of SF3B4 decreased the splicing efficiency of SPAG5 via retained

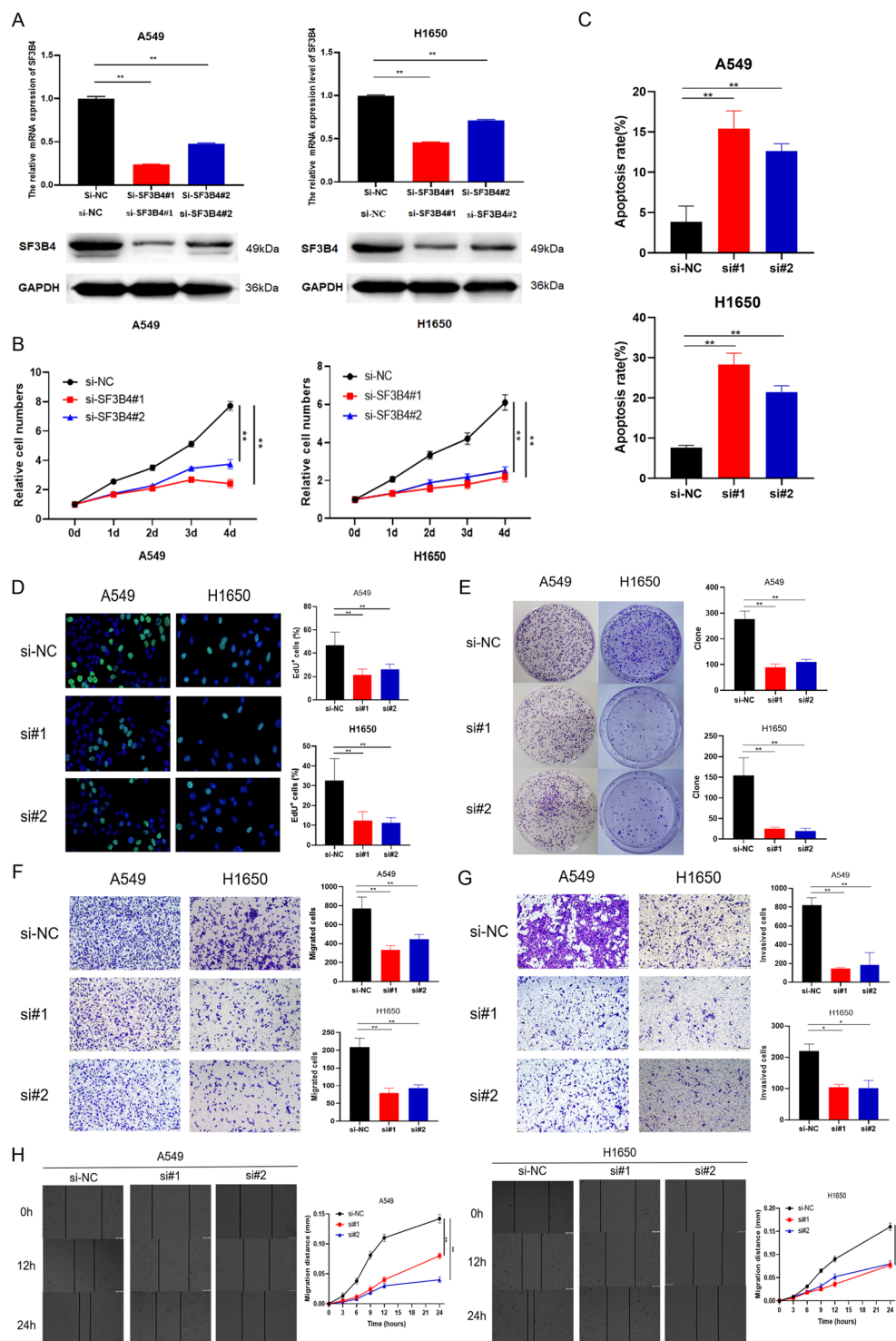


Figure 2. Effects of SF3B4 in proliferation, mobility and apoptosis of LUAD cells. **(A)** qRT-PCR and western blotting to confirm SF3B4 knockdown. **(B)** CCK8 assay on LUAD proliferation upon siRNAs transfection. **(C)** Apoptosis assay in LUAD cells. **(D)** EdU assay on proliferation capacity of LUAD cells upon siRNAs transfection. **(E)** Colony formation of LUAD cells upon siRNAs transfection. **(F, G)** Migration and invasion assays on LUAD cells upon siRNAs transfection. **(H)** Wound-healing assay on LUAD cells upon siRNAs transfection. * $P < 0.05$, ** $P < 0.01$. Original blots/gels are presented in Supplementary Raw data.

intron, leading to a reduction in SPAG5 expression²⁰. In hepatocellular carcinoma, the SF3B4 knockdown induced the inactivation of p27 by skipped exon, alternating the splicing of KLF4⁹. Since the splicing effect of SF3B4 has

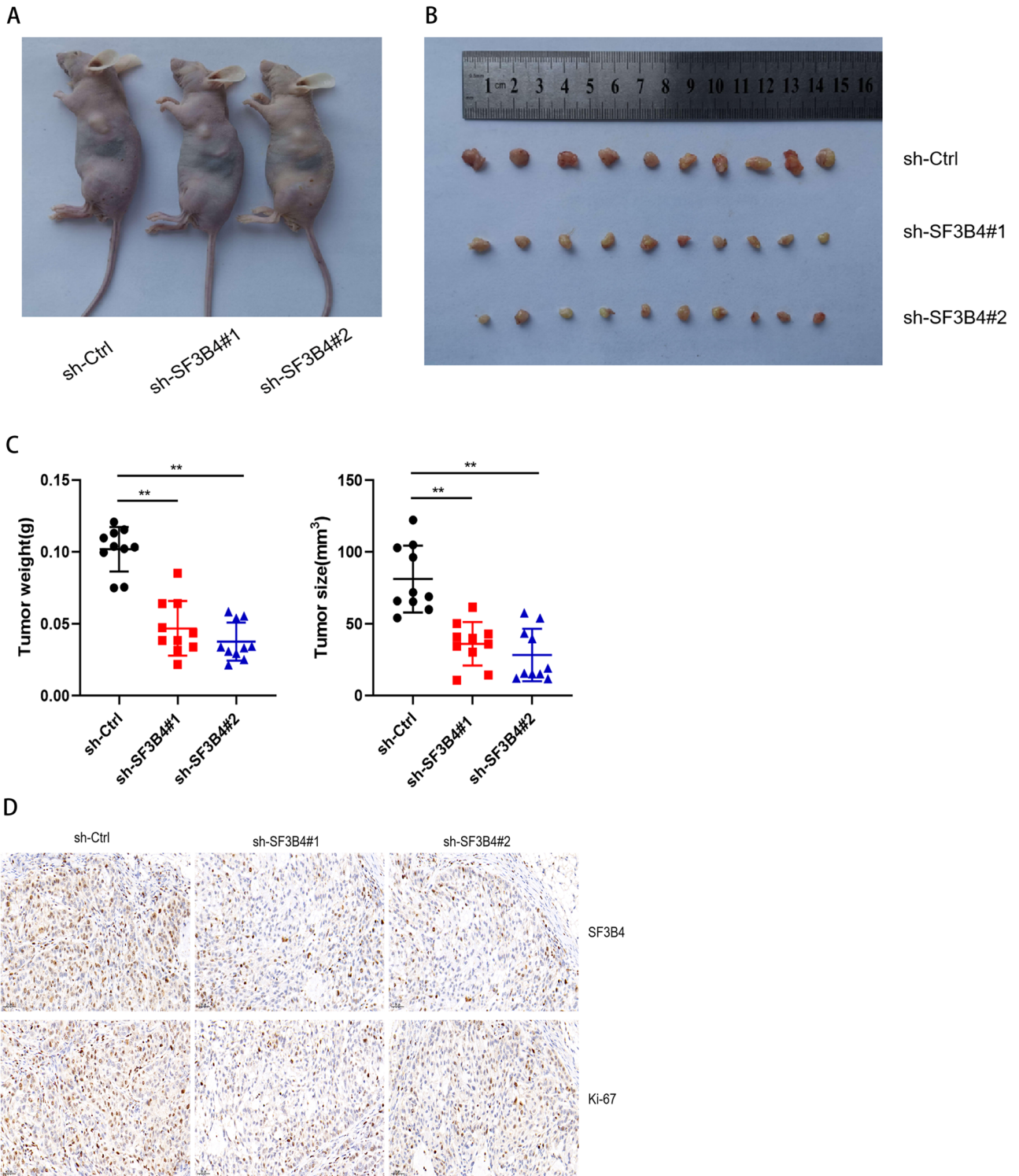


Figure 3. Effect of SF3B4 on LUAD growth in vivo. **(A)** Images of mice with tumors (n=5). **(B)** Tumors derived from sh-SF3B4 cells or control cells. **(C)** Tumor weights and size. **(D)** IHC staining results for SF3B4 and Ki-67 in tumor tissues from a mouse model. * $P < 0.05$, ** $P < 0.01$.

not been studied well in LUAD, RNA-seq was performed to screen AS events. Through rMAT analysis and RT-PCR validation, we found that an alternative splice event occurred at the 5' end of the KAT2A gene, producing a long exon. The transcript containing the long exon does not encode, resulting in the downregulation of KAT2A after SF3B4 knockdown in LUAD. Therefore, for the first time, we found that SF3B4 regulated LUAD progression via the alternative splicing of KAT2A.

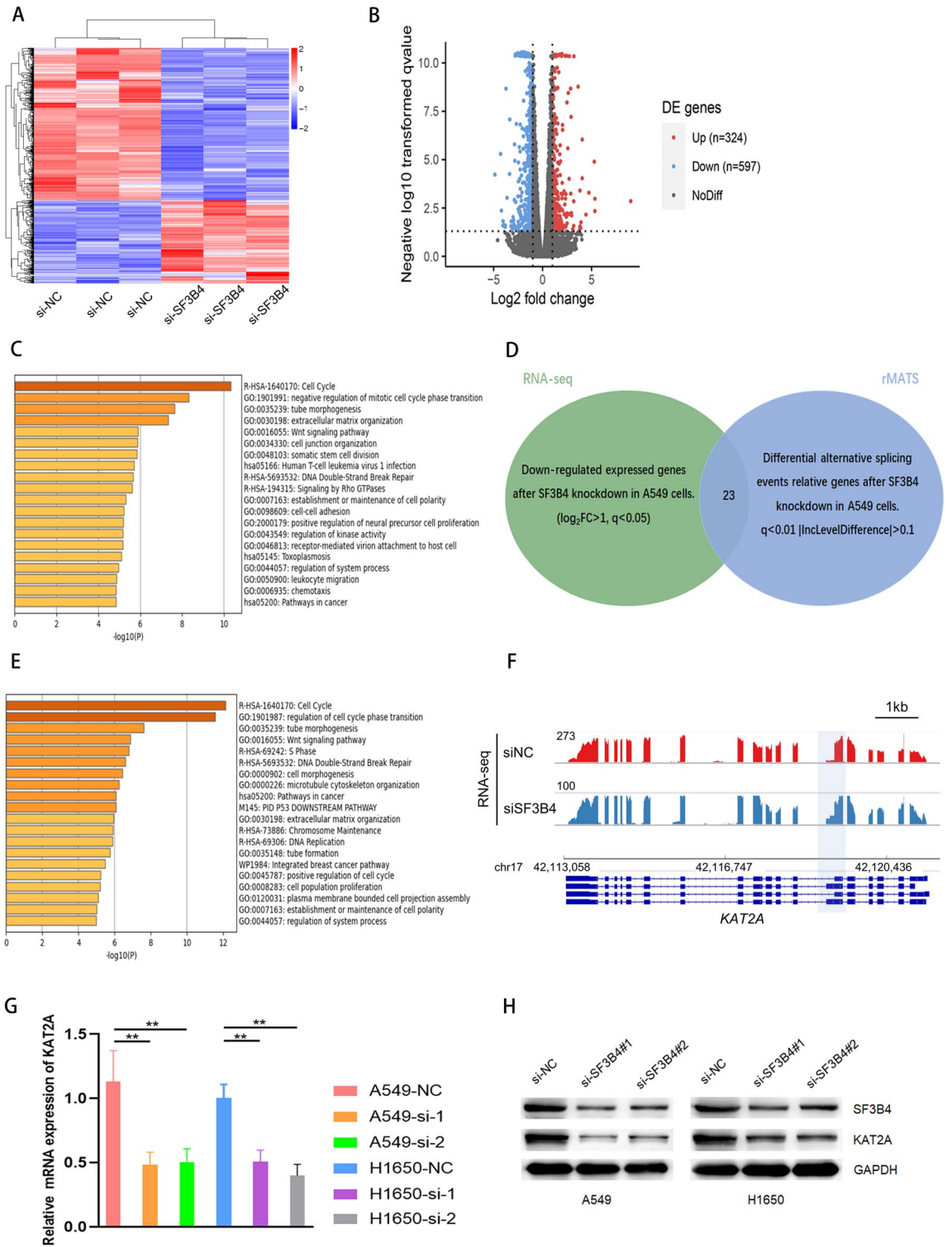
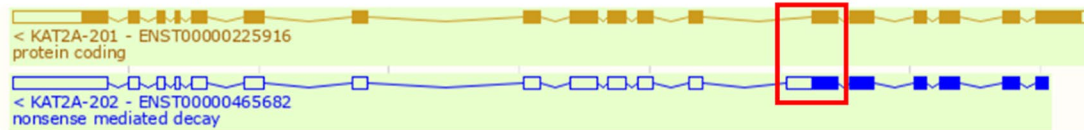


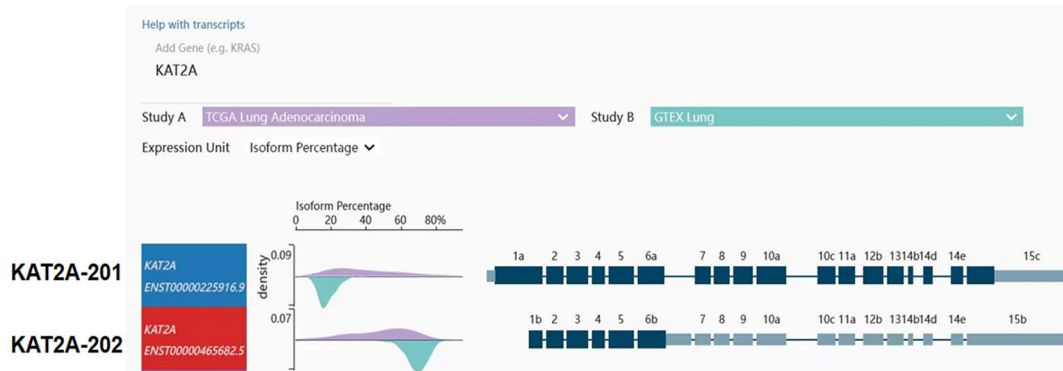
Figure 4. KAT2A is a downstream target of SF3B4. **(A,B)** Heatmap and volcano plots of DEGs from RNA-seq in A549 cells with or without SF3B4 knockdown. **(C)** GO analysis of DEGs. **(D)** Venn diagram of 3022 genes related to differential AS events upon knockdown of SF3B4. **(E)** GO analysis of downregulated DEGs **(F)** RNA-seq reads mapping to KAT2A in A549 cells upon knockdown of SF3B4. **(G,H)** qRT-PCR and western blotting of KAT2A levels upon SF3B4 knockdown in A549 cells. * $P < 0.05$, ** $P < 0.01$. Original blots/gels are presented in Supplementary Raw data.

A

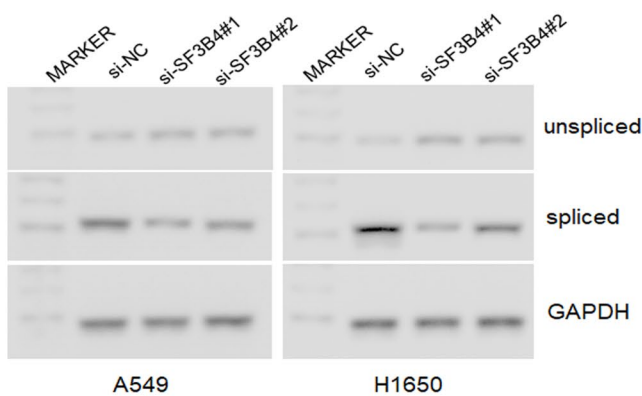
KAT2A transcripts from Ensemble website



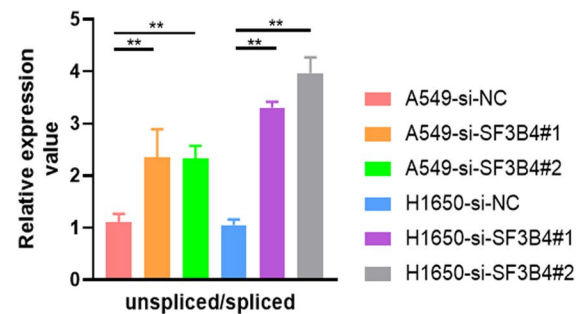
B



C



D



E

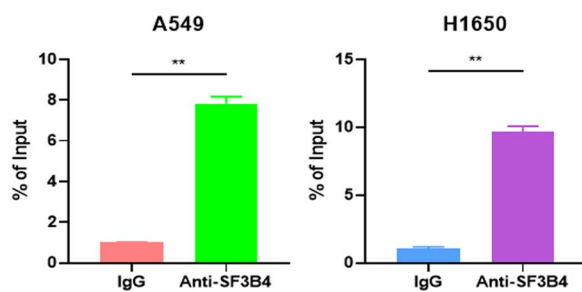


Figure 5. SF3B4 facilitates efficient splicing of KAT2A. (A) Schematic diagram on two splicing variants of KAT2A mRNA transcript. (B) Relative mRNA levels of KAT2A splicing variants in LUAD tissues (purple) and normal controls (green) from the TCGA and GTEX databases. (C,D) Relative mRNA levels of KAT2A transcripts in LUAD cells upon knockdown of SF3B4. (E) RIP-PCR in A549 and H1650 cells. * $P < 0.05$, ** $P < 0.01$.

The 5' untranslated region (5'UTR) of a mature mRNA is involved in gene regulation at the post-transcriptional level. Within a given transcriptional unit, AS is one event that induces changes to the 5'UTR sequence²¹, leading to differences in protein variant output. Selecting 5' splice-sites (5'SS) in AS plays essential roles in gene regulation, including cell proliferation, invasion, and apoptosis^{22–24}. KAT2A, a member of the N-acetyltransferase

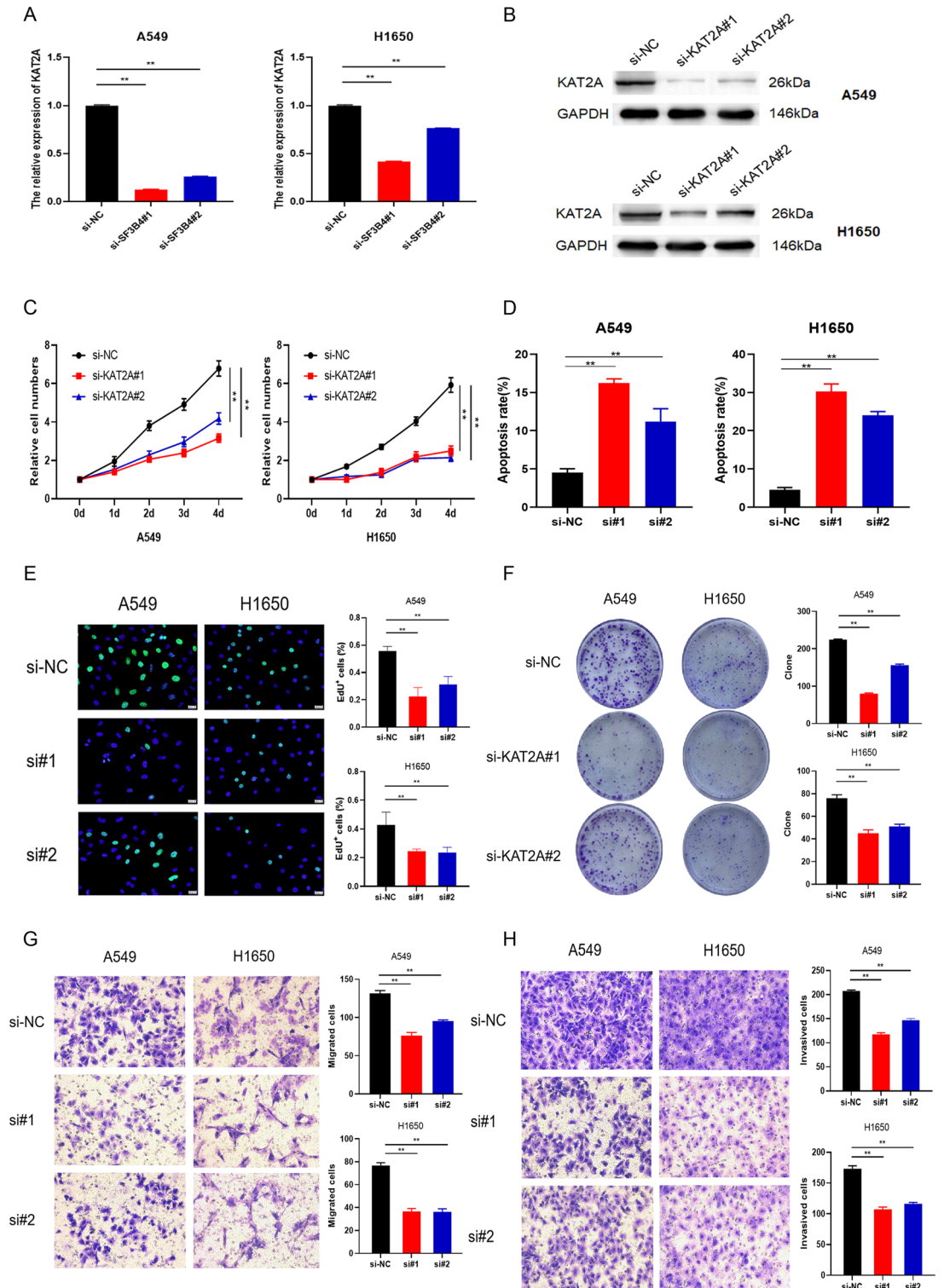


Figure 6. Effects of KAT2A on proliferation and mobility of LUAD. (A,B) qRT-PCR and western blotting on the efficiency of KAT2A knockdown by targeted siRNAs in LUAD. (C) CCK-8 test on cell proliferation. (D) Apoptosis assay on A549 and H1650 cells with or without KAT2A knockdown. (E) EdU test on cell proliferation. (F) Clonogenic assay on A549 and H1650 cells. (G, H) Transwell assays on A549 and H1650 cells. * $P < 0.05$, ** $P < 0.01$. Original blots/gels are presented in Supplementary Raw data.

superfamily, was identified as a histone acetyltransferase binding to acetyl-CoA^{25,26}. Various studies have indicated that KAT2A is an epigenetic oncogene in several malignancies^{27–29}. Besides, KAT2A has been reported

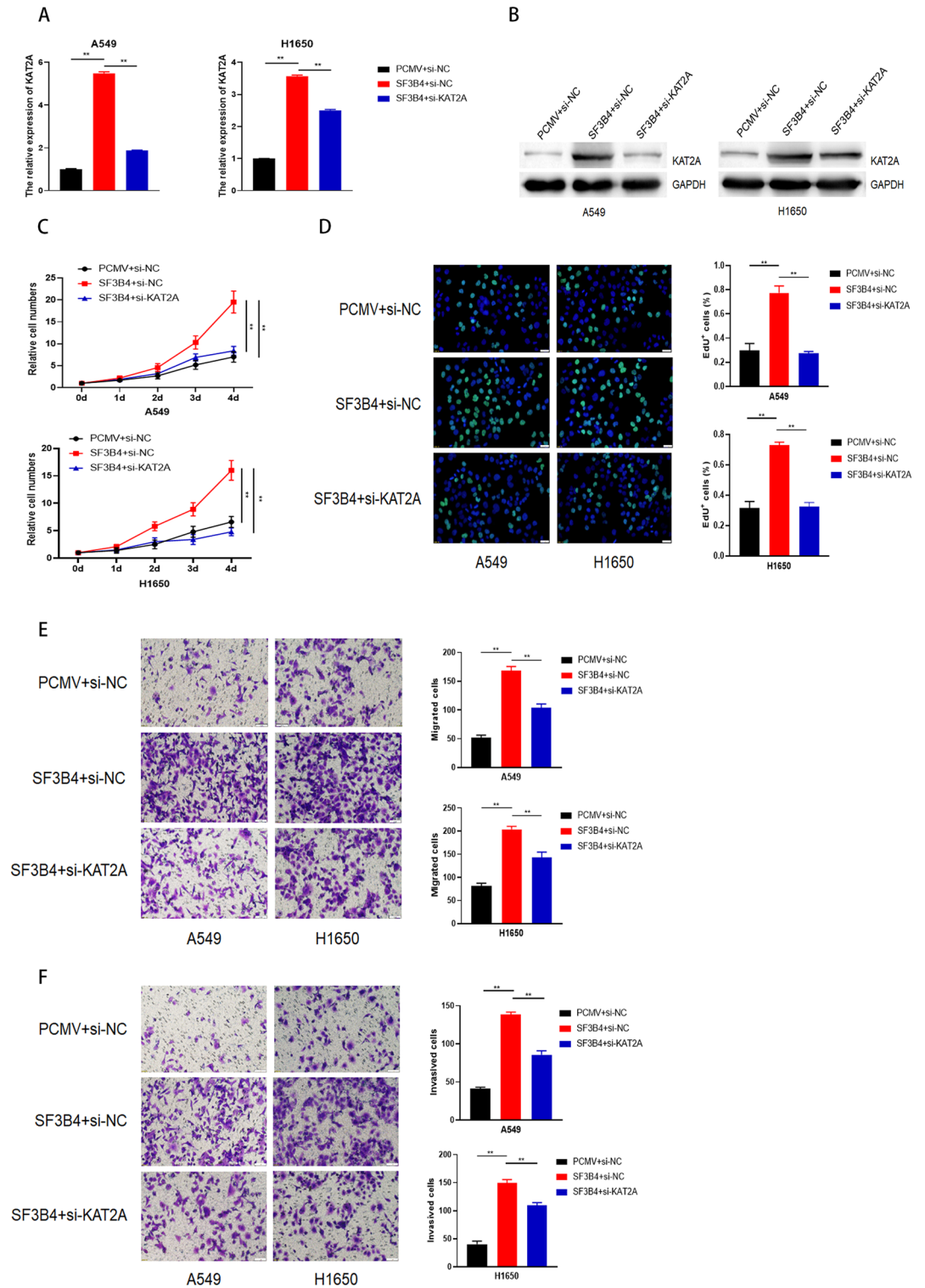


Figure 7. Effects of KAT2A on proliferation and mobility of LUAD cells with SF3B4 overexpression. **(A,B)** qRT-PCR and western blotting on the efficiency of KAT2A knockdown in LUAD cells with or without SF3B4 overexpression. **(C)** CCK-8 test on cell proliferation. **(D)** EdU test on cell proliferation of A549 and H1650 cells. **(E,F)** Transwell assays on A549 and H1650 cells upon KAT2A knockdown, with or without overexpression of SF3B4. * $P < 0.05$, ** $P < 0.01$. Original blots/gels are presented in Supplementary Raw data.

to promote stem-like cell propagation in leukemia and regulate the resistance to tamoxifen in breast cancer³⁰. However, little was known about the effects of KAT2A in LUAD. Here, we confirmed that KAT2A knockdown

decreased the capacities of LUAD cells to proliferate, invade, and migrate. The KAT2A knockdown also impaired the phenotypic changes induced upon overexpression of SF3B4.

Taken together, we explored the effects of SF3B4 in LUAD and possible mechanisms. To the best of our knowledge, SF3B4 enhanced LUAD proliferation, invasion, and migration through the alternative 5' splice Site (A5SS) of KAT2A for the first time. The KAT2A knockdown impaired the function of SF3B4 in LUAD cells. The SF3B4/ KAT2A axis could be a potential pathway to treat LUAD.

Materials and methods

Bioinformatics

The data for upregulated genes in LUAD was from GEPIA (<http://gepia.cancer-pku.cn/>). Heatmap data of cone splicing factors was from UCSC Xena (<https://xena.ucsc.edu/>). Expression of SF3B4 in normal tissues and LUAD was from TCGA and GTEX. Kaplan–Meier analysis was used to analyze the correlation of SF3B4 and OS.

Cell lines and culture

HPAEPiC, A549, and H1650 were purchased from CBTCCAS (Shanghai, China). All cells were cultured in RPMI 1640 medium (Gibco, USA) with 10% fetal bovine serum (FBS, GeneDEPOT Barker, TX, USA), 100 U/mL penicillin, and 100 µg/mL streptomycin (Biowest, Nuaille, France) at 5% CO₂, 37 °C and 95% humidity.

LUAD tissue

Primary LUAD tissues and adjacent normal lung tissues were harvested from patients in Qilu Hospital of Shandong University (Jinan, China) from May 2022 to October 2022. Prior to surgery, no patients received radiotherapy or chemotherapy. Tissues were immediately immersed in liquid nitrogen and then stayed at –80 °C. Consent was obtained from subjects. The studies were approved by the Ethics Committee of Qilu Hospital of Shandong University (KYL-202205-043-1). The clinic pathological features are summarized in Table 1.

RNA isolation and qPCR

Trizol (Invitrogen) reagent was used for total RNA extraction. A master mix kit, PrimeScript RT (Takara, RR037A), was used for cDNA synthesis. SYBR Green (Takara, RR420A) was used for qRT-PCR. For sequences for primers, see Supplementary Table 1.

Western blotting

Cell lysis was done in RIPA buffer (Beyotime Bio, Cat# P0013). The protein amount was measured with a Pierce BCA kit (Merck Millipore, Cat# 71,287). Protein samples were separated via SDS-PAGE and transferred to the PVDF membrane (Immobilon-P; Millipore, Billerica, MA, USA). After blocking with 5% BSA or fat-free milk (Amresco), the PVDF membrane was probed with primary antibodies at 4 °C overnight and then washed in TBST three times (15 min/wash). The membrane was then incubated with secondary antibodies (1:4000) at room temperature for 1 h. The antibodies information are SF3B4 (1:8000, Proteintech, 10,482-1-AP), KAT2A (1:1000, Proteintech, 66,575-1-Ig), and GAPDH (1:8000, Sigma–Aldrich, ABS16). Enhanced chemiluminescence reagent (Amersham, RPN2232) was used to expose protein bands on ImageQuant LAS 4000 (GE Healthcare Life Sciences).

RNA interference and lentiviral infection

Open reading frames of KAT2A and SF3B4 were from Vigenebio. Small interference RNAs were from GenePharma (Shanghai, China). shRNAs were constructed from vector pLKO.1-TRC. Lentivirus particles were packaged with pMD2.G and psPAX2 in HEK293 cells. LUAD cells were infected with lentivirus for 24 h. LUAD cells were then screened for 7 days in the presence of puromycin (2 µg/ml). See the sequences in Supplementary Table 2.

RNA sequencing

A549 cells were used for RNA sequencing (RNA-seq). Total mRNA was isolated with TRIzol reagent. Three replicates were produced for RNA sequencing for each sample based on the Shanghai Biotechnology Co platform. For raw sequencing data, see GSE222598 in the GEO database. An adjusted *p*-value (*p* < 0.05) and FDR < 0.01 were used as cut-offs for significantly differential expression.

Proliferation measurements

To examine cell proliferation, 3000 cells were seeded into 96-well plates. Cell viability was quantified with a CCK-8 assay kit (Invitrogen, Carlsbad, California, USA). Absorbance at 450 nm was read with a spectrophotometer (Thermo Scientific NanoDrop-2000).

Edu (Beyotime, C0071s) staining was done based on the manufacturer's protocol. Cells (1.5×10^4) in 96-well plates were incubated with Edu (1:1000 dilution) for 2 h. Cells fixation was done with 4% of paraformaldehyde. EdU immunofluorescence staining was performed using the EdU Kit (Thermo Fisher, USA) according to the manufacturer's protocol T³¹.

Colony formation

On day 1, cells (1×10^3 /well) were seeded into a 6-well plate, followed by medium change every 2 days. On day 10, colony fixation was done with methanol. Then, colonies were stained with 0.6% crystal violet and counted in Photoshop (CC 2022).

Invasion and migration

These assays were performed in transwell plates with transwell filters with 8.0 μm pore size (Corning, Cambridge, MA, USA). siRNA-transfected LUAD cells were harvested 24 h after transfection. Then, cells were washed and seeded into 24-well chambers with or without a coat of matrigel for invasion, but migration was unnecessary. Cells (1×10^5 per well) were seeded into the upper chamber in a serum-free medium. The lower chamber was filled with medium with 10% FBS. Cells were allowed to migrate or invade through pores for 12–24 h at 37 °C. At the endpoint, cells in the lower chamber were fixed in 4% paraformaldehyde. Then, cell staining was performed with 0.1% crystal violet (Sigma, C3886) at room temperature for 5 min. Cell counting was conducted under a microscope (IX71, Olympus).

Wound healing

Cells (1×10^5 /well) were seeded as monolayers in a 24-well plate. When cells were 100% confluent, a scratch line was created with a 20 μl pipette tip. Then, a medium without serum was used for cell culture. The distance between the two edges of the scratch line was monitored at 0, 12, and 24 h under a microscope (IX71, Olympus).

Immunohistochemistry

The tissue specimen was fixed with formalin and embedded with paraffin. Then, the tissue was sliced into approximately 5 μm thickness. The tissue slice was deparaffinized with xylene, rehydrated with graded ethanol, and then incubated with 3% H_2O_2 to inhibit endogenous peroxidases activity. The tissue slice was first incubated with a primary antibody at 4 °C overnight, followed by incubation with a secondary antibody for 1 h in the dark. The antibodies were anti-SF3B4 (1:200, Proteintech, 10,482-1-AP) and anti-Ki-67 (1:600, Cell Signaling Technology, 9449 T). In the end, 3,3'-diaminobenzidine tetrachloride (Sigma) chromogen solution was used to detect the amount of bound antibody. Samples were counterstained with hematoxylin, dehydrated, and mounted.

Apoptosis and cell cycle

LUAD cells were seeded as monolayers in a 6-well plate. After transfection with shSF3B4 or shControl, cells were cultured for 72 h. Cells were then harvested and stained with FITC-Annexin V and Propidium Iodide (BestBio, 4101-1). Flow cytometry (FACScan[®]; BD Biosciences) was used for analysis³².

Animal study

The study was performed based on protocol (No. SDULCLL2022-06-05) approved by the Animal Care and Use Committee of Shandong University. All methods followed relevant guidelines and regulations and were reported based on ARRIVE guidelines (<https://arriveguidelines.org>). BALB/c male nude mice (4 weeks old) were obtained from the Shanghai Laboratory Animal Center of the Chinese Academy of Sciences (Shanghai, China). Animals were randomized into two groups. One group was inoculated subcutaneously with control cells; the other was inoculated with shSF3B4 cells (5 million cells per mouse). Tumor size was calculated based on: Tumor volume = $L \times W^2 \times \pi/6$, in which W represents the shortest diameter, and L represents the longest diameter. At the endpoint, mice were euthanized with CO_2 .

RNA immunoprecipitation

RIP Kit (P0101, Genesee Biotech, Guangzhou) was used to capture the antigen after the magnetic beads were connected to the KAT2A antibody or IgG antibody. qRT-PCR was performed to detect the KAT2A mRNA level.

Statistical analysis

Statistics were performed with SPSS (version 20.0, Chicago, IL). Data plotting was done with GraphPad 7.0 (La Jolla, CA, USA). The comparison was conducted by unpaired two-tailed t-tests. All experiments had three independent replicates. Data were represented as mean \pm SD. $p < 0.05$ is statistically significant. The χ^2 -test was used to assess the relationship between expression of SF3B4 and clinical factors.

Ethics statement

All methods were carried out per the ethical standards of the responsible committee on human experimentation or with the Helsinki Declaration of 1975. The studies were approved by the Ethics Committee of Qilu Hospital of Shandong University (KYL-202205-043-1). Informed consent was obtained from patients.

Data availability

The datasets generated and analyzed during the current study are available from the corresponding author upon reasonable request.

Received: 29 March 2023; Accepted: 21 December 2023

Published online: 02 January 2024

References

1. Denisenko, T. V., Budkevich, I. N. & Zhivotovsky, B. Cell death-based treatment of lung adenocarcinoma. *Cell Death Dis.* **9**, 117 (2018).
2. Siegel, R. L., Miller, K. D. & Jemal, A. Cancer statistics, 2018. *CA Cancer J. Clin.* **68**, 7–30 (2018).
3. Nilsen, T. W. & Graveley, B. R. Expansion of the eukaryotic proteome by alternative splicing. *Nature* **463**, 457–463 (2010).
4. Wang, G. S. & Cooper, T. A. Splicing in disease: Disruption of the splicing code and the decoding machinery. *Nat. Rev. Genet.* **8**, 749–761 (2007).

5. Bonnal, S. C., López-Oreja, I. & Valcárcel, J. Roles and mechanisms of alternative splicing in cancer - implications for care. *Nat. Rev. Clin. Oncol.* **17**, 457–474 (2020).
6. Venables, J. P. *et al.* Identification of alternative splicing markers for breast cancer. *Cancer Res.* **68**, 9525–9531 (2008).
7. Venables, J. P. & Burn, J. EASI-enrichment of alternatively spliced isoforms. *Nucleic Acids Res.* **34**, e103 (2006).
8. Sheng, J. *et al.* SRSF1 modulates PTPMT1 alternative splicing to regulate lung cancer cell radioresistance. *EBioMedicine* **38**, 113–126 (2018).
9. Shen, Q. & Nam, S. W. SF3B4 as an early-stage diagnostic marker and driver of hepatocellular carcinoma. *BMB Rep.* **51**, 57–58 (2018).
10. Golas, M. M., Sander, B., Will, C. L., Lührmann, R. & Stark, H. Molecular architecture of the multiprotein splicing factor SF3b. *Science* **300**, 980–984 (2003).
11. Drozniewska, M. *et al.* Second-trimester prenatal diagnosis of Nager syndrome with a deletion including SF3B4 detected by chromosomal microarray. *Clin. Case Rep.* **8**, 508–511 (2020).
12. Lee, J. *et al.* SRSF3 depletion leads to an increase in SF3B4 expression in SNU-368 HCC cells. *Anticancer Res.* **40**, 2033–2042 (2020).
13. Kidogami, S. *et al.* SF3B4 plays an oncogenic role in esophageal squamous cell carcinoma. *Anticancer Res.* **40**, 2941–2946 (2020).
14. Kim, H. *et al.* SF3B4 depletion retards the growth of A549 non-small cell lung cancer cells via UBE4B-mediated regulation of p53/p21 and p27 expression. *Mol. Cells* **45**, 718–728 (2022).
15. Cretu, C. *et al.* Molecular architecture of SF3b and structural consequences of its cancer-related mutations. *Mol. Cell* **64**, 307–319 (2016).
16. Liu, Z. *et al.* SF3B4 is regulated by microRNA-133b and promotes cell proliferation and metastasis in hepatocellular carcinoma. *EBioMedicine* **38**, 57–68 (2018).
17. Zhou, W. *et al.* SF3B4 is decreased in pancreatic cancer and inhibits the growth and migration of cancer cells. *Tumour Biol.* **39**, 1010428317695913 (2017).
18. Denu, R. A. & Burkard, M. E. Synchronous bilateral breast cancer in a patient with nager syndrome. *Clin. Breast Cancer.* **17**, e151–e153 (2017).
19. Ding, J. *et al.* Alterations of RNA splicing patterns in esophagus squamous cell carcinoma. *Cell Biosci.* **11**, 36 (2021).
20. Li, Y. *et al.* The splicing factor SF3B4 drives proliferation and invasion in cervical cancer by regulating SPAG5. *Cell Death Discov.* **8**, 326 (2022).
21. Barrett, L. W., Fletcher, S. & Wilton, S. D. Regulation of eukaryotic gene expression by the untranslated gene regions and other non-coding elements. *Cell Mol. Life Sci.* **69**, 3613–3634 (2012).
22. Narla, G. *et al.* KLF6-SV1 overexpression accelerates human and mouse prostate cancer progression and metastasis. *J. Clin. Invest.* **118**, 2711–2721 (2008).
23. Hatami, R. *et al.* KLF6-SV1 drives breast cancer metastasis and is associated with poor survival. *Sci. Transl. Med.* **5**, 169ra112 (2013).
24. Hanoun, N. *et al.* The SV2 variant of KLF6 is down-regulated in hepatocellular carcinoma and displays anti-proliferative and pro-apoptotic functions. *J. Hepatol.* **53**, 880–888 (2010).
25. Lu, D. *et al.* KAT2A-mediated AR translocation into nucleus promotes abiraterone-resistance in castration-resistant prostate cancer. *Cell Death Dis.* **12**, 787 (2021).
26. Ouyang, C. *et al.* Deletion of Ulk1 inhibits neointima formation by enhancing KAT2A/GCN5-mediated acetylation of TUBA/ α -tubulin in vivo. *Autophagy.* **17**, 4305–4322 (2021).
27. Sun, T. T. *et al.* LncRNA GClnc1 promotes gastric carcinogenesis and may act as a modular scaffold of WDR5 and KAT2A complexes to specify the histone modification pattern. *Cancer Discov.* **6**, 784–801 (2016).
28. Bondy-Chorney, E., Denoncourt, A., Sai, Y. & Downey, M. Nonhistone targets of KAT2A and KAT2B implicated in cancer biology (1). *Biochem. Cell Biol.* **97**, 30–45 (2019).
29. Wang, Y. *et al.* The lncRNA PVT1 regulates nasopharyngeal carcinoma cell proliferation via activating the KAT2A acetyltransferase and stabilizing HIF-1 α . *Cell Death Differ.* **27**, 695–710 (2020).
30. Oh, J. H. *et al.* Elevated GCN5 expression confers tamoxifen resistance by upregulating AIB1 expression in ER-positive breast cancer. *Cancer Lett.* **495**, 145–155 (2020).
31. Diao, Y. *et al.* SF3B4 promotes ovarian cancer progression by regulating alternative splicing of RAD52. *Cell Death Dis.* **13**, 179 (2022).
32. Zhan, P. *et al.* NCAPG2 promotes tumour proliferation by regulating G2/M phase and associates with poor prognosis in lung adenocarcinoma. *J. Cell Mol. Med.* **21**, 665–676 (2017).

Author contributions

Data curation: C.E.W.; Investigation: A.L.Q.; Methodology: B.H.; Project administration: T.L.; Resources: B.H.; Validation: M.M.H.; Writing—original draft: T.L.; Writing—review & editing: T.L. All authors contributed to the article and approved the submitted version.

Competing interests

The authors declare no competing interests.

Additional information

Supplementary Information The online version contains supplementary material available at <https://doi.org/10.1038/s41598-023-50606-2>.

Correspondence and requests for materials should be addressed to T.L.

Reprints and permissions information is available at www.nature.com/reprints.

Publisher's note Springer Nature remains neutral with regard to jurisdictional claims in published maps and institutional affiliations.



Open Access This article is licensed under a Creative Commons Attribution 4.0 International License, which permits use, sharing, adaptation, distribution and reproduction in any medium or format, as long as you give appropriate credit to the original author(s) and the source, provide a link to the Creative Commons licence, and indicate if changes were made. The images or other third party material in this article are included in the article's Creative Commons licence, unless indicated otherwise in a credit line to the material. If material is not included in the article's Creative Commons licence and your intended use is not permitted by statutory regulation or exceeds the permitted use, you will need to obtain permission directly from the copyright holder. To view a copy of this licence, visit <http://creativecommons.org/licenses/by/4.0/>.

© The Author(s) 2024